Internal ocean-atmosphere variability drives megadroughts in Western North America

S. Coats[1], J. E. Smerdon[2], B. I. Cook[2,3], R. Seager[2], E. R. Cook[2], and K. J. Anchukaitis[4]

[1]Cooperative Institute for Research in Environmental Sciences, University of Colorado Boulder, Boulder, Colorado, USA, [2]Lamont-Doherty Earth Observatory, Columbia University, Palisades, New York, USA, [3]NASA Goddard Institute for Space Studies, New York, New York, USA, [4]School of Geography and Development and Laboratory of Tree Ring Research, University of Arizona, Tucson, Arizona, USA

Abstract Multidecadal droughts that occurred during the Medieval Climate Anomaly represent an important target for validating the ability of climate models to adequately characterize drought risk over the near-term future. A prominent hypothesis is that these megadroughts were driven by a centuries-long radiatively forced shift in the mean state of the tropical Pacific Ocean. Here we use a novel combination of spatiotemporal tree ring reconstructions of Northern Hemisphere hydroclimate to infer the atmosphere-ocean dynamics that coincide with megadroughts over the American West and find that these features are consistently associated with 10–30 year periods of frequent cold El Niño–Southern Oscillation conditions and not a centuries-long shift in the mean of the tropical Pacific Ocean. These results suggest an important role for internal variability in driving past megadroughts. State-of-the-art climate models from the Coupled Model Intercomparison Project Phase 5, however, do not simulate a consistent association between megadroughts and internal variability of the tropical Pacific Ocean, with implications for our confidence in megadrought risk projections.

1. Introduction

State-of-the-art coupled general circulation models (CGCMs) consistently project that much of the American West (125°W–105°W, 25°N–42.5°N) will dry over the coming decades [*Cook et al.*, 2015]. While the persistence and severity of this drying are beyond the range of observed variability (1871 to present), paleoclimate estimates suggest that drying on decadal-to-multidecadal time scales has been a prominent, albeit infrequent, feature of the Common Era (C.E.) in the American West [*Stine*, 1994; *Stahle et al.*, 2000; *Cook et al.*, 2010a; *Herweijer et al.*, 2007; *Meko et al.*, 2007; *Cook et al.*, 2016b]. Understanding the atmosphere-ocean dynamics that coincide with these so-called megadroughts is critical for determining whether CGCMs are capable of simulating multidecadal drought events and whether they do so for the correct dynamical reasons [*Coats et al.*, 2013, 2015a; *Stevenson et al.*, 2015]. Such evaluations provide confidence that future projections of drought risk derived from CGCMs adequately incorporate multidecadal hydroclimate variability [*Ault et al.*, 2014].

Characterizing megadrought dynamics are complicated by the fact that the majority of megadroughts occurred during the Medieval Climate Anomaly (MCA, approximately 850–1300 C.E. [*Jansen et al.*, 2007; *Seager et al.*, 2008]), a period for which there are no direct observations of the atmosphere-ocean system. Nevertheless, a prominent hypothesis is that the MCA megadroughts were driven by a centuries-long shift in the mean of eastern and central tropical Pacific sea surface temperatures (SSTs) toward persistently cold conditions (hereinafter tropical Pacific mean shift [*Herweijer et al.*, 2007; *Seager et al.*, 2008; *Graham et al.*, 2007]). It has been proposed that the tropical Pacific mean shift arose as an ocean dynamical thermostat response [*Clement et al.*, 1996] to relatively high radiative forcing [*Crowley*, 2000], and the hypothesis has been tested by using a range of reconstruction techniques and proxy networks [*Seager et al.*, 2007, 2008; *Graham et al.*, 2007, 2011; *Mann et al.*, 2009; *Emile-Geay et al.*, 2013], as well as pseudoproxy experiments [*Smerdon et al.*, 2016; *Wang et al.*, 2014]. These studies, however, are largely inconclusive, and there is insufficient evidence to support or disprove the hypothesis that megadroughts are exogenously forced or driven by a tropical Pacific mean shift [*Cook et al.*, 2016b]. In support of the latter assertion, available reconstructions of tropical Pacific SSTs disagree on the association between megadroughts and the tropical Pacific (Figure S1 and Text S1, section A in the supporting information).

In this study we do not attempt another reconstruction. Instead, we infer the past state of the dominant modes of Northern Hemisphere atmosphere-ocean variability by using the spatial patterns they impose on multiple, existing, and independent tree ring-based reconstructions of Northern Hemisphere hydroclimate variability. Specifically, we use the instrumental record (1871–2005 C.E.) of the El Niño–Southern Oscillation (ENSO—Niño3.4 index), Atlantic Multidecadal Oscillation (AMO [*Enfield et al.*, 2001]), Pacific Decadal Oscillation (PDO [*Mantua et al.*, 1997]), and North Atlantic Oscillation (NAO) to define the patterns of hydroclimate associated with these modes of variability (hereinafter, modes of variability will to refer to the ENSO, AMO, PDO, and NAO), in isolation and in combination, in the tree ring reconstructed North American Drought Atlas (NADA [*Cook et al.*, 2014]), Monsoon Asia Drought Atlas (MADA [*Cook et al.*, 2010b]), and newly developed Old World Drought Atlas (OWDA [*Cook et al.*, 2016a]). We then identify preinstrumental analogues of these patterns in the first combined analysis of the three drought atlases to determine the most likely atmosphere-ocean state for each year back to 1000 C.E. (hereinafter the climate analogues framework—see section 3 for description and Text S2, sections A–C and Figures S2, S3, S4, S5, and S6 for method validation). Importantly, there are multiple levels of independence between the observations of these modes of variability and the drought atlases and between each individual drought atlas (see Text S1, section B for further discussion). Our analyses therefore allow us to address two questions: (1) what is the state of the ENSO, AMO, PDO, and NAO during megadroughts in the American West? and (2) are the characteristics of these modes of variability during megadroughts consistent with internal variability or do they require radiative forcing?

2. Data

Reconstructed PDSI data are from three sources. The first is the updated NADA version 2a, with improved spatial coverage and resolution [*Cook et al.*, 2014]. The data are reconstructed on a 0.5° latitude-longitude grid of JJA average PDSI values using more than 1600 tree ring chronologies. The second is the OWDA [*Cook et al.*, 2016a], also reconstructed on a 0.5° latitude-longitude grid of JJA average PDSI values using 106 tree ring chronologies from across Europe. Both the NADA and OWDA are used over the period 1000–2005 C.E. The third is the MADA [*Cook et al.*, 2010b], reconstructed on a 2.5° latitude-longitude grid of JJA average PDSI values using 327 tree ring chronologies. The MADA is employed over the period 1250–2005 C.E. when there is sufficient proxy sample depth over the spatial range. All three reconstructed PDSI data sets have been regridded to a common 2.5° latitude-longitude grid for our analyses.

All climate indices are calculated for the period of 1871–2005 C.E. using sea surface temperature (SST) observations from the National Oceanic and Atmospheric Administration (NOAA) extended reconstructed SST data set (NOAA ERSSTv3b [*Smith and Reynolds*, 2003]) or surface pressure from the NOAA twentieth century reanalysis [*Compo et al.*, 2011]. Both data sources are fully independent of the aforementioned tree ring reconstructions. The Niño3.4 index was calculated by averaging December-January-February (DJF) SST over the region 170°W–120°W, 5°S–5°N (hereinafter, the state of ENSO will refer to the state of the Niño3.4 index). The PDO was evaluated by calculating the empirical orthogonal functions (EOFs) of SST over the extratropical Pacific basin (60°W–75°E, 20°N–90°N), and subsequently taking the DJF average of the principle component time series corresponding to the first EOF [*Mantua et al.*, 1997] (positive values corresponding to a warm tropical and North Pacific Ocean). The AMO was calculated by averaging JJA Atlantic SSTs over the region 80°W–0°E, 0°N–60°N, subtracting the global average of JJA SSTs between 60°S–60°N and then 10 year low-pass filtering [*Enfield et al.*, 2001]. The NAO was calculated from the twentieth century reanalysis as the sea level pressure difference between the Subtropical (Azores) High (37.82°N, 25.75°W) and the Subpolar Low (65.08°N, 22.73°W) for the November-December-January-February-March (NDJFM) period. Sensitivity of the methodology and results to the choice of three different observational data sets is addressed in Text S2, section D.

3. Climate Analogues Framework

The following steps describe the climate analogues framework, with the final subsection providing a brief description of the method validation (the full method validation can be found in Text S2, sections A–C).

3.1. Sorting the Dynamics

The instrumental record (1871–2005 C.E.) is segmented into years that are in the top (positive), middle (neutral), and bottom (negative) third of the full distribution of the ENSO, AMO, PDO, and NAO indices.

3.2. Defining Impact Maps

Hydroclimate composites are produced from a simplified version of the collection of drought atlases where each spatiotemporal grid point is assigned 1 for wet (positive PDSI) and 0 for dry. The composites are calculated for all years that fall in the positive, neutral, or negative state of each mode (12 in total—three for each of the four modes of variability). The positive ENSO composite, for instance, is a composite of the three drought atlases over all years in the instrumental record with a positive ENSO state (top third). The composites are also calculated for all combinations of two-to-four modes. For instance, composites are calculated for all years with a positive ENSO state and each of the nine states of the other three modes (e.g., positive ENSO and positive AMO; two-mode combinations), as well as all combinations of three and four modes using the same logic. These composites are estimates of the impact of the four modes of variability on hydroclimate in the drought atlases (hereinafter impact maps). Specifically, each impact map determines if the positive, negative, or neutral state of each mode, or some combination of the states of multiple modes, tends to produce wetting or drying at each spatial grid point. Because of standardization employed in the drought atlases, wetting or drying in each impact map is relative to the period 1928–1978 C.E., 1928–1978 C.E., and 1951–1989 C.E.in the NADA, OWDA, and MADA, respectively. To encourage sufficient sampling within the impact maps we only employ impact maps for which at least 4 years within the instrumental record have the defined atmosphere-ocean state. This restriction yields a total of 154 impact maps (of 255 possible).

All impact maps are calculated by using JJA PDSI with the atmosphere-ocean state defined by the preceding DJF average ENSO or PDO indices, the preceding NDJFM average NAO index, or the contemporaneous JJA average AMO index. PDSI is an integrated metric of soil moisture with 10–18 months of inherent persistence. JJA PDSI over the American West, for instance, primarily reflects variability in cool season (winter and early spring) precipitation [*St. George et al.*, 2010]. The dominant hydroclimate impacts of these modes of variability are thus likely to be captured despite the varying seasonality of impacts across the Northern Hemisphere. For instance, in Figure S2, the canonical impacts of the four modes of variability are clearly evident in the impact maps.

3.3. Dynamical Time Series

For each year back to 1000 C.E. the pattern of hydroclimate in the drought atlases is compared to each of the 154 impact maps using a centered pattern correlation statistic (CPCS [*Santer et al.*, 1995]), a measure of the similarity of patterns equivalent to a Pearson's linear correlation coefficient in space rather than in time. For the period after 1250 C.E., the impact map that best matches the spatial pattern of reconstructed hydroclimate across all three drought atlases in a given year (highest CPCS) defines the atmosphere-ocean state for that year. For 1000 C.E.–1249 C.E., however, the spatial pattern of reconstructed hydroclimate is compared to the impact maps only over the NADA and OWDA regions (as the MADA begins in 1250 C.E.).

Not all of the 154 impact maps provide a value for the state of all four modes. The impact map that corresponds to just a positive ENSO state, for instance, does not provide a value for the state of the PDO, AMO, and NAO. For years in which the chosen impact map (highest CPCS) corresponds to a one-, two-, or three-mode combination, secondary impact maps are also chosen in order to provide values for the modes that were not a part of the highest CPCS combination. To do so, the impact map with the next highest CPCS and a value for at least one of the missing modes is chosen as the secondary impact map. This process continues until a value for all four modes is determined in a given year. In each case the secondary impact maps have to be dynamically consistent with the first impact map, and each other (for instance, if the primary impact maps were for a positive ENSO state the secondary impact maps cannot have a neutral or negative ENSO state). For the climate analogues framework completed herein the 5th, 50th, and 95th percentiles of the CPCS between the drought atlases and the impact maps that define the atmosphere-ocean state in each year are 0.20, 0.30, and 0.49, respectively.

3.4. Time Series Filtering

The dynamical time series derived from the climate analogues framework are 10 year low-pass filtered using a 10-point Butterworth filter to elucidate the decadal-to-multidecadal variability of the four modes of variability.
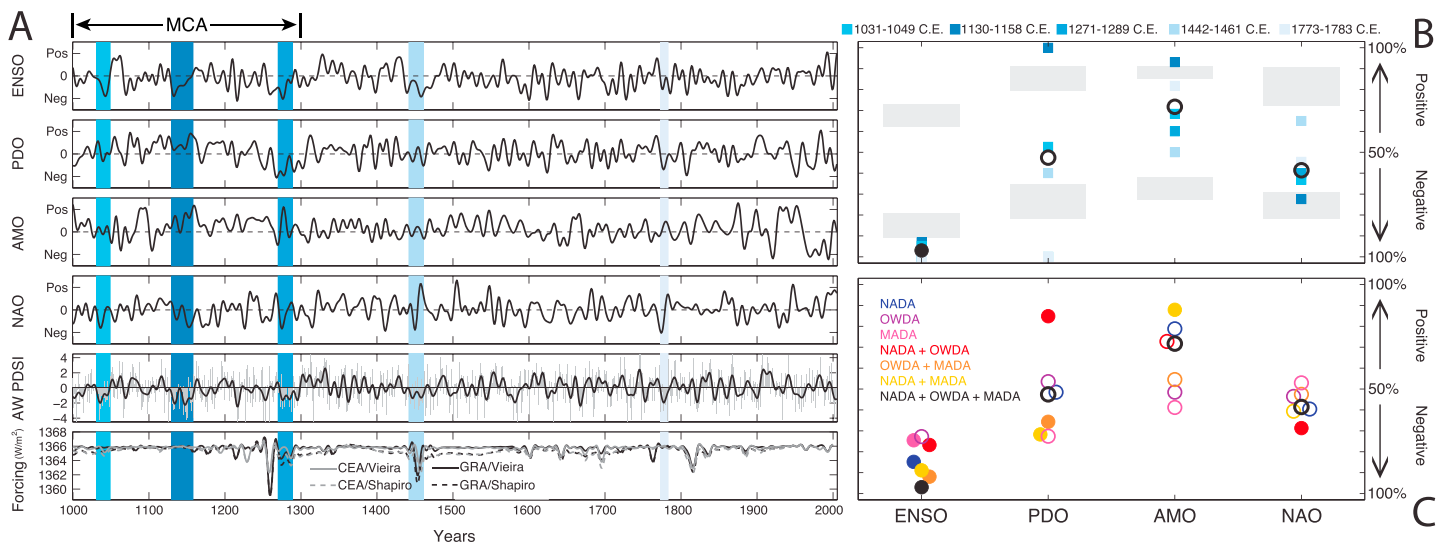
Figure 1. (a) Time series of estimated ENSO, PDO, AMO, and NAO states with the five identified megadroughts denoted by the colored regions (the darker blues denote more persistent and severe megadroughts). The time series show a 10 year low-pass filtered (10-point Butterworth filter) version of the estimated states using the results from the climate analogues framework (section 3). If the time series reaches the "positive" hash on the vertical axis (this label denotes the maximum value the time series can attain) then all of the individual years contributing to the 10 year low-pass filtered value would be positive. The start and end of the MCA (1000–1300 C.E.) is marked by the vertical bars at the top of the figure. The second to bottom figure shows the American West PDSI time series from the NADA, in which the megadroughts were identified. The bottom figure shows the combinations of two solar (Vieira [*Vieira and Solanki*, 2009] and Shapiro [*Shapiro et al.*, 2011] and two volcanic (GRA [*Gao et al.*, 2008 and CEA [*Crowley*, 2000]) forcing data sets for the period of 1000–2000 C.E. (b) The association between the five identified megadroughts and the time series of estimated ENSO, PDO, AMO, and NAO states in Figure 1a. For associations at 100% positive, every year of the identified drought has a value that is positive (and vice versa for 100% "negative"). The colored squares are the results for each of the five megadroughts considered individually. The shaded regions in Figure 1b are the 95% significance level for these five megadroughts using a distribution and autocorrelation preserving bootstrapping method to test statistical significance (Text S2, section G)—the different lengths of each of the five megadroughts results in the range of the 95% significance level. The circles show values for all five identified megadroughts considered collectively (values correspond to all years identified as being megadrought years), with the filled circles being those associations that are significant at the 95% level. (c) The values for all five identified megadroughts considered collectively but calculated using subsets of the full Northern Hemisphere dendroclimatic reconstructions. All of these indicate a statistically significant association between megadroughts and ENSO except for the case in which the OWDA is considered alone.

3.5. Method Validation

Four 500 year control simulations [*Taylor et al.*, 2012] are used in a pseudoproxy context to test the climate analogues framework (Text S2, sections A–C). The method is significantly skillful for the ENSO and NAO, and this behavior is not highly model-dependent; however, skill is limited for the AMO and PDO. The inability to reproduce the AMO and PDO appears to be related to difficulty constraining their impacts on hydroclimate over the Northern Hemisphere given the long time scales of variability inherent to these modes and the short 135 year (1871–2005 C.E.) training interval. Nevertheless, model representation of the hydroclimate impacts of the PDO and AMO is poor [*Coats et al.*, 2015b], and the pseudoproxy-derived skill for these modes may be a pessimistic representation of actual skill. Additionally, the climate analogues framework is found to be relatively insensitive to choice of observational data set (Text S2, section D and Figure S7) and to changes in the tree ring site distribution and density over the analysis period (Text S2, section E, Figure S8, and Table S2).

4. Results and Conclusions

Consistent with prior analyses [*Coats et al.*, 2013, 2015a], we define a drought as beginning with two consecutive years of negative hydroclimate anomalies and ending with two consecutive years of positive hydroclimate anomalies, with the sum of hydroclimate anomalies between the start and end of each drought determining the rank. Focus is limited to the five most severe and persistent (highest-ranked) droughts over the American West in the NADA for the period of 1000–2005 C.E. (hereinafter megadroughts). Using the output of the climate analogues framework (Figure 1a) we assess the percentage of megadrought years that have positive or negative values of the ENSO, PDO, AMO, and NAO (Figure 1b). Megadroughts over the American West are consistently and significantly tied to periods with a higher than average frequency of cold ENSO conditions, with 96% of megadrought years having negative ENSO values in Figure 1a. The significance
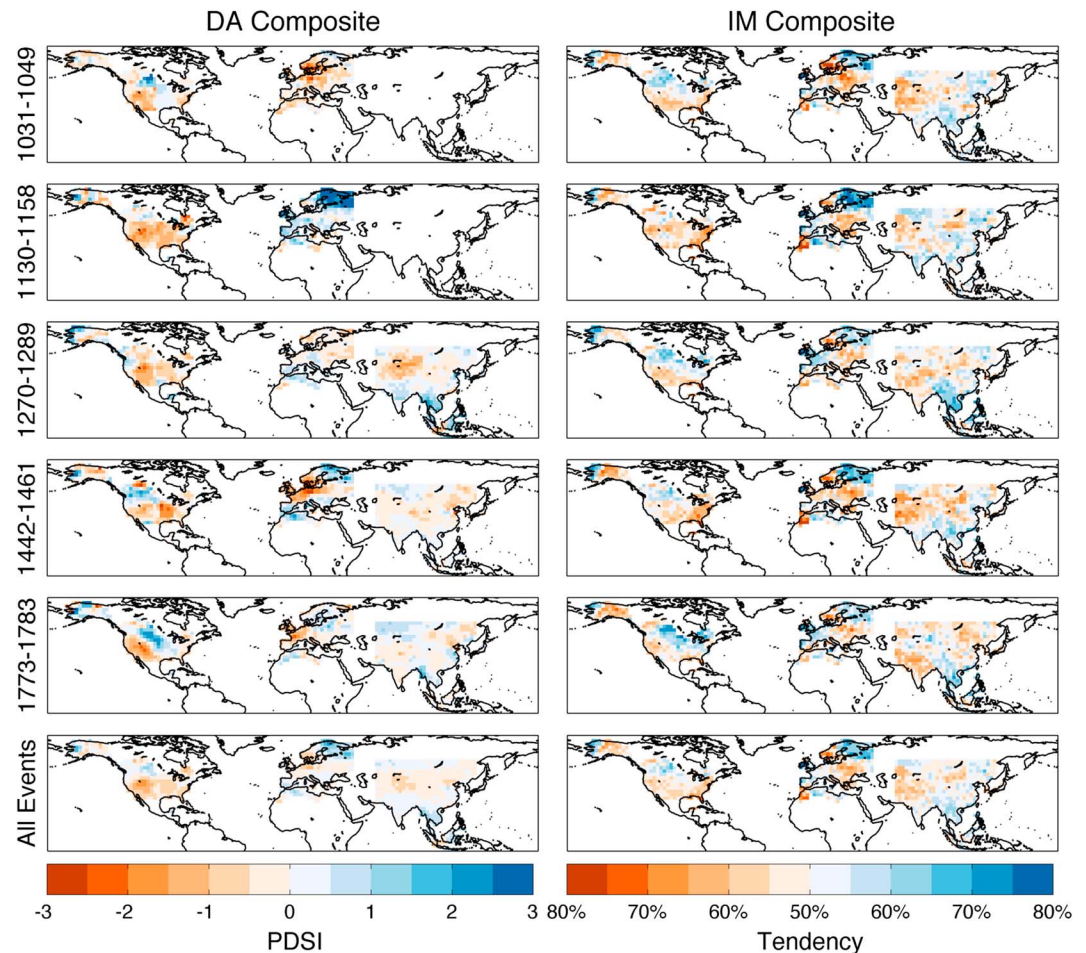
Figure 2. (left column) Drought atlas and (right column) impact map composites for the five identified megadrought periods. The drought atlas composites are the actual hydroclimate patterns during each megadrought. The impact map composites (see Text S1, section C for further discussion) are the hydroclimate patterns during each megadrought implied by the atmosphere-ocean states estimated from the climate analogues framework in Figure 1. Composites are shown for each of the five identified megadroughts (dates on the left side of each row) and all five megadroughts considered collectively ("All Events"—values correspond to all years identified as being megadrought years).

of this association is found to be present regardless of the underlying regions employed in the climate analogues framework (with the only exception being when just the OWDA is used—Figure 1c), providing confidence that the association is robust and not dependent on ENSO teleconnections to the NADA, the drought atlas in which the megadroughts were identified. Instead, megadroughts over the American West occur as a part of hemisphere-scale hydroclimate patterns (Figure 2a) that are characteristic of a negative ENSO state (Figure 2b and Text S1, section C).

The three most severe and persistent megadroughts in the American West over the last millennium occurred during the MCA (Figure 1). While the limitations of the tree ring record constrain our analyses to the period after 1000 C.E., all five of the most severe and persistent megadroughts would fall within the MCA in the broad sense [*Coats et al.*, 2015a, 2016; *Seager et al.*, 2008]. MCA megadrought severity and clustering, along with strong coupling of American West hydroclimate to tropical Pacific SSTs and a hypothesized ocean dynamical thermostat response to high radiative forcing, have led to speculation that there was a tropical Pacific mean shift over the extent of the MCA [*Herweijer et al.*, 2007; *Seager et al.*, 2007; *Graham et al.*, 2007]. The tropical Pacific, however, does not appear to have persistently cold conditions during the MCA, or more generally during any MCA-length (300 year) period (Figure 1a), contradicting the hypothesis that there was a radiatively forced tropical Pacific mean shift. Confidence in this conclusion requires that the
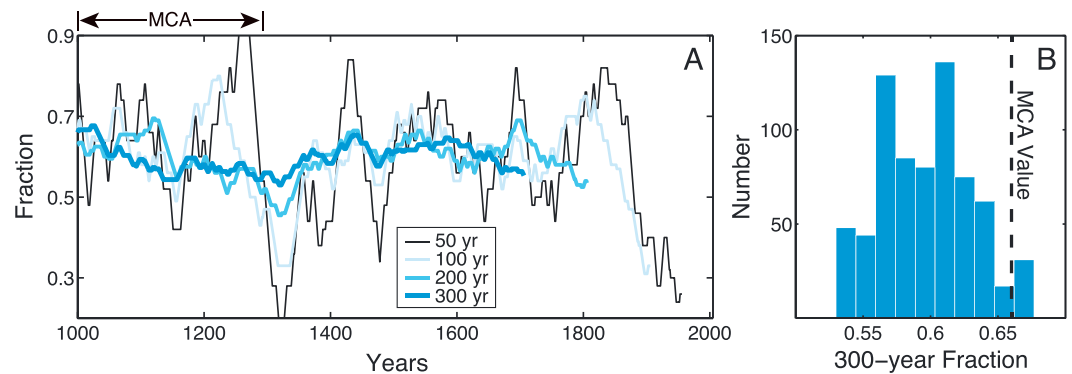
Figure 3. (a) Fraction of years with a negative value in the time series of ENSO states from Figure 1a for sliding windows of 50, 100, 200, and 300 year length. The horizontal axis shows the first year of each window. (b) Histogram of the fraction of years in each 300 year segment (length of the MCA) with a negative ENSO value. The value corresponding to the MCA (1000–1300 C.E.) is plotted as the vertical dashed line.

climate analogues framework can capture 300 year tropical Pacific mean shifts similar to what was suggested to have occurred during the MCA [*Mann et al.* [2009]], and pseudoproxy experiments demonstrate that this is the case (Figure S9 and Text S2, section F).

Shorter 10–30 year periods with a higher than average frequency of cold ENSO conditions (hereinafter, tropical Pacific cold states will be used to specifically refer to periods with a higher than average frequency of cold ENSO conditions), however, are a relatively consistent feature of last-millennium ENSO variability (Figure 1a). It is these features that coincide with the five identified megadroughts (Figure 1b). While the MCA has a high incidence of 10–30 year tropical Pacific cold states, the temporal clustering is not unique when compared to other 300 year periods. The 300 year period beginning in the late sixteenth century, for instance, also has a high incidence of tropical Pacific cold states (Figures 1a and 3a). Likewise, the fraction of negative ENSO values (Figure 1a) during the MCA is not unique when compared to other 300 year periods (95th percentile, Figure 3b). Finally, the three tropical Pacific cold states that coincide with the MCA megadroughts are not the most exceptional of the last millennium when ranked by the number of consecutive negative ENSO years (they are the 4th, 5th, and 14th ranked).

Tropical Pacific cold states during the MCA are neither more prevalent nor exceptional in character, suggesting that other modes of atmosphere-ocean variability may have played a secondary role in determining the severity and clustering of MCA megadroughts. There were warm conditions in the Atlantic during the MCA, as the AMO is predominantly positive from ~1100–1300 C.E. (Figure 1a). In fact, the MCA is the 300 year period with the highest inferred occurrence of years with both a negative ENSO state and positive state of the AMO. A potential mechanism would involve warm tropical North Atlantic SSTs and associated local and interbasin tropospheric heating driving equatorward descending flow over the American West that suppresses summer precipitation [*Kushnir et al.*, 2010] and modulating ENSO-driven tropical Pacific precipitation and associated teleconnections during winter [*Enfield et al.*, 2001; *Kushnir et al.*, 2010]. This background drying and modulated ENSO impact during the MCA would then allow 10–30 year tropical Pacific cold states to produce particularly severe megadroughts. Important caveats, however, are that the AMO was not positive during the early part of the MCA (Figure 1a), and it is difficult for the climate analogues framework to reproduce the state of the AMO because of poor sampling of such low-frequency modes over the 135 year training interval (Figures S3, S4, S5, and S6 and Text S2, sections A–C). Further research on the state of the AMO during the MCA will be necessary to provide confidence in this result, but time series modeling [*Coats et al.*, 2016] and model-based analyses have suggested an important role for the AMO in driving drying over North America during the MCA ([*Feng et al.*, 2008; *Oglesby et al.*, 2011]—also see Text S2, section D).

With regard to the forced versus internal origins of megadroughts, the 10–30 year tropical Pacific cold states that coincide with megadroughts (Figure 1) appear to be well within the range of internal variability. This includes the tropical Pacific cold states during the MCA, which were neither more persistent nor more prevalent than those in other 300 year periods and, which were associated with average solar and volcanic
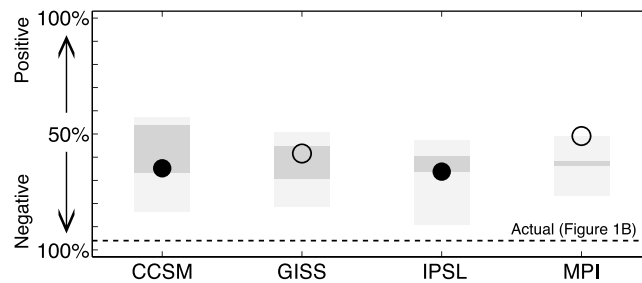
Figure 4. The association between the five most persistent and severe droughts over the American West (megadroughts) and the ENSO state in four preindustrial control simulations from CGCMs (Table S1). The circles show the values for all five identified megadroughts considered collectively (values correspond to all years identified as being megadrought years in each simulation), with the filled circles being those associations that are significant at the 95% level. The shaded regions show the associations implied by the climate analogues frameworks computed as a part of the pseudoproxy experiments in Text S2, section A. The dark gray shaded region is the 25th to 75th percentiles of these associations with the light gray shaded region representing the full range. The dashed line is the value for the actual climate analogues framework from Figure 1b.

conditions (the average forcing during MCA megadroughts is approximately equal to the 1000–2000 C.E. mean—Figure 1a, bottom and Table S3). When taken together, these findings are either inconsistent with an ocean dynamical thermostat during the MCA [*Mann et al.*, 2009] or the forced response was substantially smaller than internal variability. Nevertheless, radiative forcing changes were weaker than in the late twentieth century (e.g., Figure 1a, bottom), and therefore, the ocean dynamical thermostat may indeed be a response of the climate system to stronger radiative forcing. A persistently positive AMO during the MCA, also may not have required radiative forcing if the AMO is associated with long time scales of predominantly internal variability, although the origins and character of

the AMO are being actively debated [*Clement et al.*, 2015; *Zhang et al.*, 2016]. If this is the case then no externally forced atmosphere-ocean dynamics are needed to explain megadroughts, including the clustering and severity of megadroughts during the MCA, with internal variability likely playing an important role.

These results have implications for the evaluation of CGCMs and their regional hydroclimate projections of economically, culturally, and agriculturally significant areas of the American West. CGCMs consistently simulate megadroughts driven by internal variability, but under a range of different atmosphere-ocean states [*Coats et al.*, 2013, 2015a; *Stevenson et al.*, 2015]. There are, however, some CGCMs that simulate a significant association between megadroughts and the tropical Pacific Ocean (e.g., CCSM and IPSL in Figure 4). Nevertheless, the consistency of this association is much weaker than in the real world, according to this analysis, even when considering the uncertainty of the climate analogues framework (Figure 4). While we are less confident in a role for the AMO in driving background drying during the MCA, most CGCMs also lack a realistic AMO and associated hydroclimate impacts over the American West [*Coats et al.*, 2015b]. Fundamentally, these conclusions imply that CGCM-based hydroclimate projections may not account for the full range of potential future trajectories in the Pacific and likely also the Atlantic Oceans, and their associated hydroclimate impacts, and thus may struggle to accurately represent megadrought risk in the near-term future.

References

Ault, T. R., J. E. Cole, J. T. Overpeck, G. T. Pederson, and D. M. Meko (2014), Assessing the risk of persistent drought using climate model simulations and paleoclimate data, *J. Clim.*, doi:10.1175/JCLI-D-11-00732.1.

Clement, A., K. Bellomo, L. N. Murphy, M. A. Cane, T. Mauritsen, G. Rädel, and B. Stevens (2015), The Atlantic Multidecadal Oscillation without a role for ocean circulation, *Science*, 350(6258), 320–324.

Clement, A. C., R. Seager, M. A. Cane, and S. E. Zebiak (1996), An ocean dynamical thermostat, *J. Clim.*, 9, 2190–2196.

Coats, S., J. E. Smerdon, R. Seager, B. I. Cook, and J. F. González-Rouco (2013), Megadroughts in southwest North America in millennium-length ECHO-G simulations and their comparison to proxy drought reconstructions, *J. Clim.*, 26, 7635–7649.

Coats, S., J. E. Smerdon, B. I. Cook, and R. Seager (2015a), Are simulated megadroughts in the North American southwest forced?, *J. Clim.*, doi:10.1175/JCLI-D-14-00071.1.

Coats, S., B. I. Cook, J. E. Smerdon, and R. Seager (2015b), North American Pancontinental droughts in model simulations of the Last Millennium, *J. Clim.*, 28, 2025–2043.

Coats, S., J. E. Smerdon, K. B. Karnauskas, and R. Seager (2016), The improbable but unexceptional occurrence of megadrought clustering in the American West during the Medieval Climate Anomaly, *Environ. Res. Lett.*, 11(7), 074025.

Compo, G. P., et al. (2011), Review Article The Twentieth Century Reanalysis Project, Publications, Agencies and Staff of the U.S. Department of Commerce. Paper 254.

Cook, B. I., J. E. Smerdon, R. Seager, and E. R. Cook (2014), Pan-continental droughts in North America over the Last Millennium, *J. Clim.*, 27, 383–397, doi:10.1175/JCLI-D-13-00100.1.

Cook, B. I., T. R. Ault, and J. E. Smerdon (2015), Unprecedented 21st-century drought risk in the American Southwest and Central Plains, *Sci. Adv.*, *1*, e1400082, doi:10.1126/sciadv.1400082.

Cook, B. I., E. R. Cook, J. E. Smerdon, R. Seager, A. P. Williams, S. Coats, D. W. Stahle, and J. V. Díaz (2016a), North American megadroughts in the Common Era: Reconstructions and simulations, *Wiley Interdiscip. Rev. Clim. Change*, *7*(3), 411–432.

Cook, E. R., R. Seager, M. A. Cane, and D. W. Stahle (2007), North American drought: Reconstructions, causes, and consequences, *Earth Sci. Rev.*, *81*(1–2), 93–134.

Cook, E. R., R. D. D'Arrigo, and K. J. Anchukaitis (2009), Tree ring 500 year ENSO index reconstructions, NOAA/NCDC Paleoclimatology Program.

Cook, E. R., R. Seager, R. R. Heim Jr., R. S. Vose, C. Herweijer, and C. Woodhouse (2010a), Megadroughts in North America: Placing IPCC projections of hydroclimatic change in a long-term palaeoclimate context, *J. Quat. Sci.*, *25*, 48–61, doi:10.1002/jqs.1303.

Cook, E. R., K. J. Anchukaitis, B. M. Buckley, R. D. D'Arrigo, G. C. Jacoby, and W. E. Wright (2010b), Asian monsoon failure and megadrought during the last millennium, *Science*, *328*, 486–489.

Cook, E. R., et al. (2016b), Old world megadroughts and pluvials during the Common Era, *Sci. Adv.*, doi:10.1126/sciadv.1500561.

Crowley, T. J. (2000), Causes of climate change over the past 1000 years, *Science*, *289*, 270–277.

Emile-Geay, J., K. M. Cobb, M. E. Mann, and A. T. Wittenberg (2013), Estimating central equatorial Pacific SST variability over the past millennium. Part II: Reconstructions and implications, *J. Clim.*, *26*, 2329–2352, doi:10.1175/JCLI-D-11-00511.1.

Enfield, D. B., A. M. Mestas-Nuñez, and P. J. Trimble (2001), The Atlantic multidecadal oscillation and its relation to rainfall and riverflows in the continental U.S, *Geophys. Res. Lett.*, *28*, 2077–2080, doi:10.1029/2000GL012745.

Feng, S., R. J. Oglesby, C. M. Rowe, D. B. Loope, and Q. Hu (2008), Atlantic and Pacific SST influences on medieval drought in North America simulated by the Community Atmospheric Model, *J. Geophys. Res.*, *113*, D11101, doi:10.1029/2007JD009347.

Gao, C., A. Robock, and C. Ammann (2008), Volcanic forcing of climate over the last 1500 years: An improved ice-core based index for climate models, *J. Geophys. Res.*, *113*, D2311, doi:10.1029/2008JD010239.

George, S. S., D. M. Meko, and E. R. Cook (2010), The seasonality of precipitation signals embedded within the North American Drought Atlas, *Holocene*, *20*, 983–988.

Graham, N. E., et al. (2007), Tropical Pacific–mid-latitude teleconnections in medieval times, *Clim. Change*, *83*, 241–285.

Graham, N. E., C. M. Ammann, D. Fleitmann, K. M. Cobb, and J. Luterbacher (2011), Support for global climate reorganization during the "Medieval Climate Anomaly, *Clim. Dyn.*, *37*, 1217–1245.

Herweijer, C., R. Seager, E. R. Cook, and J. Emile-Geay (2007), North American droughts of the Last Millennium from a gridded network of tree-ring data, *J. Clim.*, *20*, 1353–1376, doi:10.1175/JCLI4042.1.

Hirahara, S., M. Ishii, and Y. Fukuda (2014), Centennial-scale sea surface temperature analysis and its uncertainty, *J. Clim.*, *27*, 57–75.

Jansen, E., et al. (2007), Palaeoclimate, in *Climate Change, The Physical Science Basis. Contribution of Working Group I to the Fourth Assessment Report of the Intergovernmental Panel on Climate Change*, edited by S. Solomon et al., pp. 433–497, Cambridge Univ. Press, Cambridge, U. K., and New York.

Kaplan, A., M. Cane, Y. Kushnir, A. Clement, M. Blumenthal, and B. Rajagopalan (1998), Analyses of global sea surface temperature 1856–1991, *J. Geophys. Res.*, *103*, 567–18, doi:10.1029/97JC01736.

Kushnir, Y., R. Seager, M. Ting, N. Naik, and J. Nakamura (2010), Mechanisms of tropical Atlantic SST influence on North American precipitation variability, *J. Clim.*, *23*, doi:10.1175/2010JCLI3172.1.

Li, J., et al. (2013), El Niño modulations over the past seven centuries, *Nat. Clim. Change*, *3*, 822–826, doi:10.1038/nclimate1936.

MacDonald, G. M., and R. A. Case (2005), Variations in the Pacific Decadal Oscillation over the past millennium, *Geophys. Res. Lett.*, *32*, L08703, doi:10.1029/2005GL022478.

Mann, M. E., Z. Zhang, S. Rutherford, R. S. Bradley, M. K. Hughes, D. Shindell, C. Ammann, G. Faluvegi, and F. Ni (2009), Global signatures and dynamical origins of the Little Ice Age and Medieval Climate Anomaly, *Science*, *27*, 1256–1260.

Mantua, N. J., S. R. Hare, Y. Zhang, J. M. Wallace, and R. C. Francis (1997), A Pacific interdecadal climate oscillation with impacts on salmon production, *Bull. Am. Meteorol. Soc.*, *78*, 1069–1079.

McCabe, G. J., M. A. Palecki, and J. L. Betancourt (2004), Pacific and Atlantic ocean influences on multidecadal drought frequency in the United States, *Proc. Natl. Acad. Sci. U.S.A.*, *101*(12), 4136–4141.

Meko, D., C. A. Woodhouse, C. A. Baisan, T. Knight, J. J. Lukas, M. K. Hughes, and M. W. Salzer (2007), Medieval drought in the upper Colorado River Basin, *Geophys. Res. Lett.*, *34*, L10705, doi:10.1029/2007GL029988.

Oglesby, J. R., S. Feng, Q. Hu, and C. Rowe (2011), Medieval drought in North America: The role of the Atlantic multidecadal oscillation, in *PAGES News*, vol. 19, pp. 18–19, PAGES International Project Office, Bern, Switzerland.

Ortega, P., F. Lehner, D. Swingedouw, V. Masson-Delmotte, C. C. Raible, M. Casado, and P. Yiou (2015), A model-tested North Atlantic Oscillation reconstruction for the past millennium, *Nature*, *523*(7558), 71–74.

Santer, B. D., K. E. Taylor, T. M. L. Wigley, J. E. Penner, P. D. Jones, and U. Cubasch (1995), Towards the detection and attribution of an anthropogenic effect on climate, *Clim. Dyn.*, *12*, 77–100.

Schrieber, T., and A. Schmitz (2000), Surrogate time series, *Phys. D*, *142*, 346–382.

Seager, R., N. Graham, C. Herweijer, A. L. Gordon, Y. Kushnir, and E. Cook (2007), Blueprints for Medieval hydroclimate, *Quat. Sci. Rev.*, *26*, 2322–2336, doi:10.1016/j.quascirev.2007.04.020.

Seager, R., R. Burgman, Y. Kushnir, A. Clement, E. Cook, N. Naik, and J. Miller (2008), Tropical Pacific forcing of North American medieval megadroughts: Testing the concept with an atmosphere model forced by coral-reconstructed SSTs, *J. Clim.*, *21*, 6175–6190.

Shapiro, A. I., W. Schmutz, E. Rozanov, M. Schoell, M. Haberreiter, A. V. Shapiro, and S. Nyeki (2011), A new approach to the long-term reconstruction of the solar irradiance leads to large historical solar forcing, *Astron. Astrophys.*, *529*, A67.

Smerdon, J. E., A. Kaplan, D. Chang, and M. N. Evans (2010), A pseudoproxy evaluation of the CCA and RegEM methods for reconstructing climate fields of the Last Millennium, *J. Clim.*, *23*, 4856–4880, doi:10.1175/2010JCLI3328.1.

Smerdon, J. E., S. Coats, and T. R. Ault (2016), Model-dependent spatial skill in pseudoproxy experiments testing climate field reconstruction methods for the Common Era, *Clim. Dyn.*, doi:10.1007/s00382-015-2684-0.

Smith, T. M., and R. W. Reynolds (2003), Extended reconstruction of global sea surface temperatures based on COADS data (1854–1997), *J. Clim.*, *16*, 1495–1510.

Stahle, D. W., E. R. Cook, M. K. Cleaveland, M. D. Therrell, D. M. Meko, H. D. Grissino-Mayer, E. Watson, and B. H. Luckman (2000), Tree-ring data document 16th century megadrought over North America, *Eos Trans. AGU*, *81*(12), 121–125, doi:10.1029/00EO00076.

Stevenson, S., A. Timmermann, Y. Chikamoto, S. Langford, and P. DiNezio (2015), Stochastically generated North American megadroughts, *J. Clim.*, *28*, 1865–1880.

Stine, S. (1994), Extreme and persistent drought in California and Patagonia during medieval time, *Nature*, *369*, 546–549.

Taylor, K. E., R. J. Stouffer, and G. A. Meehl (2012), An overview of CMIP5 and the experiment design, *Bull. Am. Meteorol. Soc.*, *93*, 485–498.

Tierney, J. E., N. J. Abram, K. J. Anchukaitis, M. N. Evans, C. Giry, K. H. Kilbourne, C. P. Saenger, H. C. Wu, and J. Zinke (2015), Tropical sea surface temperatures for the past four centuries reconstructed from coral archives, *Paleoceanography*, *30*, 226–252, doi:10.1002/2014PA002717.

Trouet, V., J. Esper, N. E. Graham, A. Baker, J. D. Scourse, and D. C. Frank (2009), Persistent positive North Atlantic Oscillation mode dominated the medieval climate anomaly, *Science*, *324*, 78–80, doi:10.1126/science.1166349.

Vance, T. R., J. L. Roberts, C. T. Plummer, A. S. Kiem, and T. D. van Ommen (2015), Interdecadal Pacific variability and eastern Australian megadroughts over the last millennium, *Geophys. Res. Lett.*, *42*, 129–137, doi:10.1002/2014GL062447.

Vieira, L. E. A., and S. Solanki (2009), Evolution of the solar magnetic flux on time scales of years to millennia, *Astron. Astrophys.*, doi:10.1051/0004-6361/200913276.

Wang, J., J. Emile-Geay, D. Guillot, J. E. Smerdon, and B. Rajaratnam (2014), Evaluating climate field reconstruction techniques using improved emulations of real-world conditions, *Clim. Past*, *10*, 1–19, doi:10.5194/cp-10-1-2014.

Zhang, R., R. Sutton, G. Danabasoglu, T. L. Delworth, W. M. Kim, J. Robson, and S. G. Yeager (2016), Comment on "The Atlantic Multidecadal Oscillation without a role for ocean circulation", *Science*, *352*(6293), 1527–1527.